ACS APPLIED MATERIALS & INTERFACES

Research Article

www.acsami.org

Controlled Topography Change of Subdiffraction Structures Based on Photosensitive Polymer Films Induced by Surface Plasmon Polaritons

Tobias König,[†,‡] Vladimir V. Tsukruk,[‡] and Svetlana Santer*[,†]

[†]Department of Experimental Physics, Institute of Physics and Astronomy, Karl-Liebknecht Strasse 24/25, University of Potsdam, 14476 Potsdam, Germany

[‡]School of Materials Science and Engineering, Georgia Institute of Technology, Atlanta, Georgia 30332, United States

Supporting Information

ABSTRACT: We discuss the controlled subdiffraction modulations of photosensitive polymer films that are induced by surface plasmon interference in striking contrast to well-known conventional microscopic gratings. The near-field light intensity patterns were generated at the nanoslits fabricated in a silver layer with the photosensitive polymer film placed above. We observed that the topographical modulations can be excited only when the polarization is perpendicular to the nanoslits. Moreover, we have shown that light with certain wavelengths resulted in a characteristic topographical pattern with the periodicity three times smaller than the wavelength of incoming light. A combination of experimental observations with simulations showed that the unique subdiffraction topographical patterns are caused by constructive interference between two counter-propagating surface plasmon waves generated at neighboring nanoslits in the metal layer beneath the photosensitive polymer film. The light intensity distribution was simulated to demonstrate strong dependency upon the slit array periodicity as well as wavelength and polarization of incoming light.

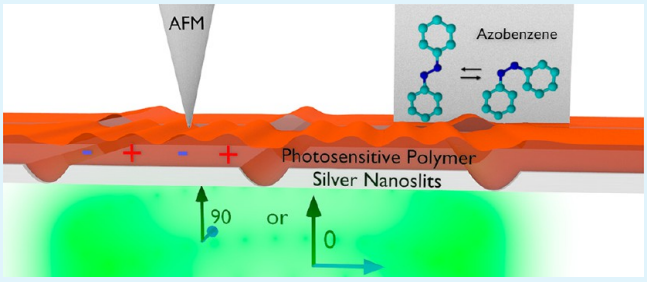

KEYWORDS: *azobenzene photosensitive polymer films, surface plasmon polaritons, silver nanoslits*

INTRODUCTION

Light-induced formation of periodic polymeric materials is a popular approach to create complex patterned materials via local polymerization, materials transfer, local scission, or photoisomerization reactions.[1−5] Scaling down light-induced periodic polymer structures well below the diffraction limit is a great challenge. In this way, it is possible to squeeze light into subwavelength dimensions by exploiting surface plasmon phenomena and thus overcoming the diffraction limit.[6−10] Surface plasmon polaritons are electromagnetic waves bound to a metal−dielectric interface and are excited by light.[11−13] They are generated when incoming light triggers collective oscillations of the electron charges at the metal−dielectric interfaces. In the polaritons formation, the frequency of the electron charge osciallations remains the same as the incoming light, while the wavelength becomes significantly smaller, thus facilitating subdiffraction light-assisted nanolithography.[11] It is possible to squeeze light into subwavelength dimensions and thus overcome the diffraction limit.[14−16] One of the intriguing and rapidly growing applications of this phenomenon is SP-assisted nanolithography.[7,17−20] In this approach, a near-field intensity pattern generated at metallic subwavelength structures is printed into a topography of photosensitive polymer film.

SP-assisted nanolithography has been used as an alternative method to optical scanning probe techniques for direct visualization of the near-field intensity pattern. It has been demonstrated that the near-field light intensity pattern can be imprinted in the polymer film photochemically (i.e., using conventional photoresists where irreversible changes within the polymer film are induced by light).[6,7] An alternative is to utilize the photophysical reaction of polymer films on irradiation, where a polymer mass will migrate from areas of high intensity to those of low intensity or vice versa.[21] In this case, the light-induced changes can be reversible as by changing the distribution of light intensity on the polymer film, one is able to alternate repeatedly between different topographical states.[20,22−25]

It has been known that proper light irradiation of thin azobenzene-containing polymer films with UV interference patterns generates surface relief gratings,[26−28] which are modulations of the polymer film topography that closely follow the corresponding intensity distribution generated by interference lithography with periodicity dictated by the light

Received: February 25, 2013
Accepted: May 23, 2013
Published: May 23, 2013

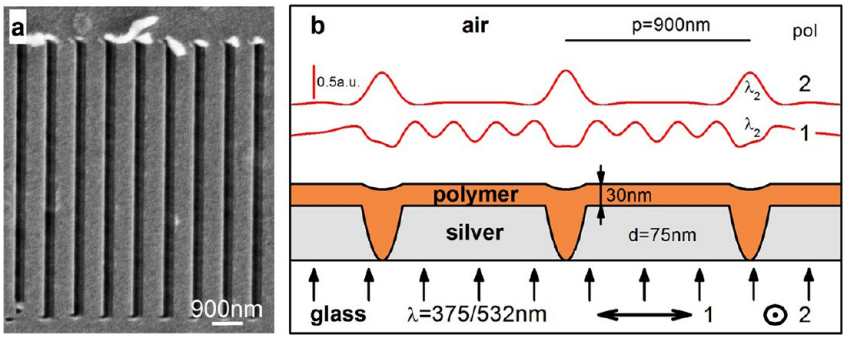

Figure 1. (a) SEM image of the nanoslit array (900 nm periodicity). (b) Red lines represent an intensity distribution of the calculated near-field pattern generated at the polymer−air interface during irradiation of the nanoslits from below with the 532 nm wavelength of light. The subscripts 1 and 2 mark the intensity for the different polarizations of incoming light, perpendicular (pol = 0°, marked as 1) and parallel (pol =9 0°, marked as 2), with respect to the direction of the nanoslits.

wavelength. On the molecular level the origin of such peculiar behavior is a photoisomerization of azobenzene molecules that undergo reversible transitions from trans- to the cis-configuration during irradiation with UV light.[29] The properties of the azobenzene molecules in trans and cis form differ significantly; for instance, the size of the molecules changes by almost a factor of 2, requiring for the cis configuration more free volume, and the dipole moment changes from 0D for the trans (the more stable configuration) to 3D for the cis-isomer. Moreover, during multiple photoisomerisation steps the azobenzene molecules rotate in such a way that their long axis is aligned perpendicularly to the electrical field vector. All these local changes in the properties of the azobenzene containing polymer result in a material flow and thus global deformation of the film.[30−32] Remarkably, the formation of very fine gratings can also be achieved using the interference of two counter-propagating surface plasmon waves generated at the bottom of nanoslits within a metal layer.[23] In this way, it is possible to overcome the diffraction limit and produce stable structural features in polymer films as small as one-third of the incoming wavelength. This study was the first step to map two counter-propagating surface plasmon wave as an interference pattern. However, the topographical pattern could be altered significantly by different parameters of optical stimuli, such as wavelengths, polarization or polymer film thickness, which opens the use for manifold controllable surface pattern with a high spatial resolution. Such controllable manipulation requires further insight into how these parameters might affect the polymer−light−metal interactions.

In this paper, we present a further study of the near-field topographical patterning of polymer films produced by an array of nanoslits within a metal layer as a function of irradiation wavelength and polarization of the incoming light. We focus on simulation of the corresponding optical phenomena with use of a finite-difference time-domain (FDTD) simulation method to study the plasmonic slit modes and the corresponding surface charge distribution at different wavelengths, geometrical parameters, and polarization angles.

EXPERIMENTAL SECTION

Fabrication of the Metallic Nanostructures. The 75 nm silver (Ag) layer was deposited on a cleaned glass substrate by a thermal evaporation technique. Parallel nanoslits were fabricated using AFM scratching. The nanofabrication procedure was performed in atomic force microscopy (AFM) contact-mode (INTEGRA, NT-MDT, Russia) utilizing a silicon nitride tip (Nanosensors) with a resonance frequency of around 300 kHz and a spring constant of around k = 45 N/m.[33] The direction of scratching was kept perpendicular to the long axis of the cantilever and the load force was adjusted to be 31 μN in order to remove the silver layer completely. The periodicity of an array of parallel nanoslits was kept at 900 nm. The periodicity was chosen to be much longer than the surface plasmon wavelength to leave sufficient enough space for interference. The surface morphology was recorded in tapping mode using tips from LOT-Oriel (APP-ACL uncoated cantilever, resonance frequency of around ∼150 kHz, spring constant of around ∼25 N/m).

Photosensitive Polymer. The synthesis of the azobenzene-containing poly(ethylene imine)-(Methyl red, Na salt) is described in detail in previous publications.[20,34] The absorption spectra and chemical structure of the supramolecular material containing azobenzene are shown in the Supporting Information (Figure S-1). The 30 nm polymer film was prepared by spin coating 5 mg/mL MeOH solution at 3000 rpm for 1 min on top of the Ag nanostructured substrate. An increase in the humidity from 50 to 98% flattens any inscribed topographical patterns associated with the underlying metal structure.

Experimental Setup. The homemade experimental setup used in this paper is described elsewhere.[20−25] Briefly, we combined an optical setup for the generation of surface plasmons and AFM in order to simultaneously acquire topography changes during light irradiation of the sample from the backside. In this study, we apply irradiation of two wavelengths of 375 or 532 nm, having intensities of I_{375} = 90 mW cm^{-2} and I_{532} = 80 mW cm^{-2}. The polarization of incoming light was changed between parallel (pol=90°) and perpendicular (pol = 0°) to the nanoslits. The optical setup (light plan) is attached in the Supporting Information Figure S-2.

FDTD Simulations. Simulation of the near-field intensity distributions, extinction spectra, and surface charge distributions were done using the commercial software from Lumerical Solutions Inc. (FDTD Solutions, Version 7.5.7). The permittivity of the metals was taken from Hagemann et al. (CRC Handbook of Chemistry and Physics).[35] The silver permittivity was fitted over the simulation bandwidth with four coefficients and a RMS error of 0.203. The permittivity of the polymer film at two wavelengths, ε_{375} = 1.803+i0.880 and ε_{532} = 3.670+i0.163, was determined by ellipsometry (Nanofilm EP3). The glass permittivity (ε_{glass} = 2.155) was taken from Palik[36] and assumed to be constant over the simulation bandwidth.

RESULTS AND DISCUSSION

Figure 1a shows parallel nanoslits of 900 nm periodicity fabricated in a silver layer. The nanoslits were scratched down to the glass surface and have a parabolic profile (Figure 1b). The width is a uniform 200 nm along the whole length (10 μm) of the slit at the metal surface. The removed material is deposited at the end of the nanoslits. The measurements were performed in the middle of the nanoslit-structures in order to avoid edge effects. The topography of the nanoslits was still

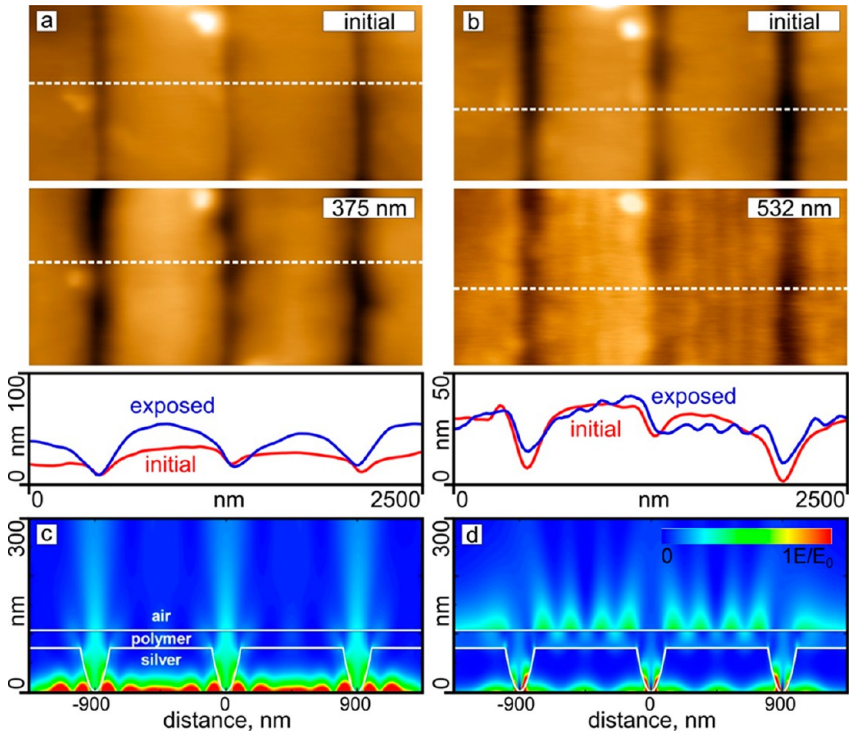

Figure 2. AFM micrographs of the polymer topography recorded before (above picture) and after 34 min of irradiation at (a) 375 and (b) 532 nm. The direction of polarization points perpendicular to the nanoslits in both cases. The AFM cross-sections underneath show the initial profile before irradiation (red line) and after irradiation (blue line). (c, d) Corresponding image plots showing the distributions of the near-field intensity pattern. Red in c and d indicates maximum intensity.

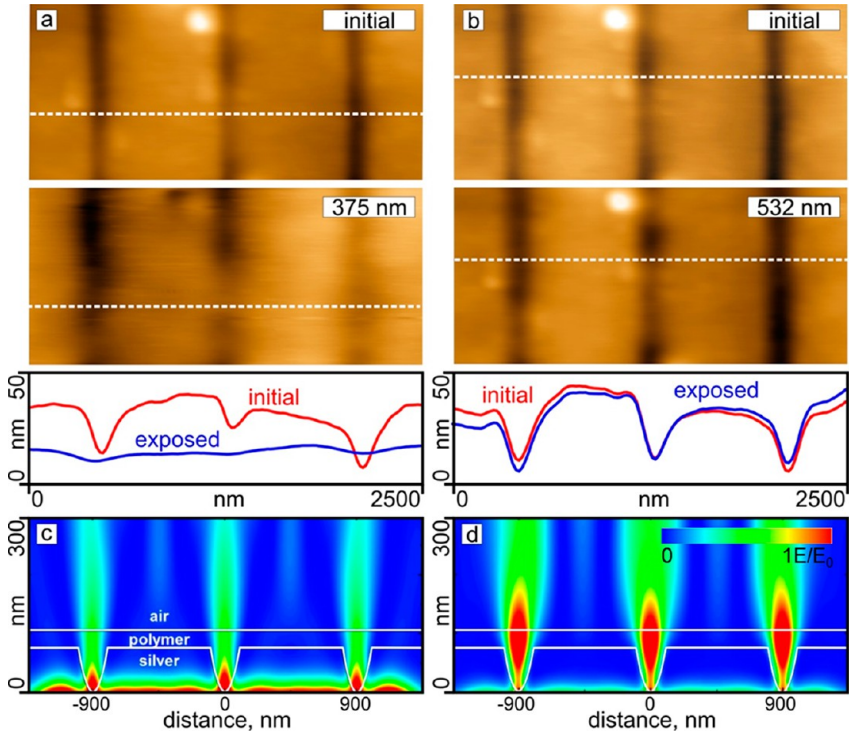

Figure 3. AFM images of the polymer topography before (top) and after (bottom) 34 min of irradiation at (a) 375 and (b) 532 nm. The direction of polarization is parallel to the nanoslits in both cases. The corresponding AFM cross-section shows that polymer material fills the nanoslits during irradiation. For the shorter wavelength the topography flattens almost completely, whereas irradiation with longer wavelength results in only a moderate decrease of the nanoslit depth. (c, d) Corresponding image plots showing the distributions of the near-field intensity pattern. Red in c and d indicates maximum intensity.

dx.doi.org/10.1021/am400712r | ACS Appl. Mater. Interfaces 2013, 5, 6009−6016

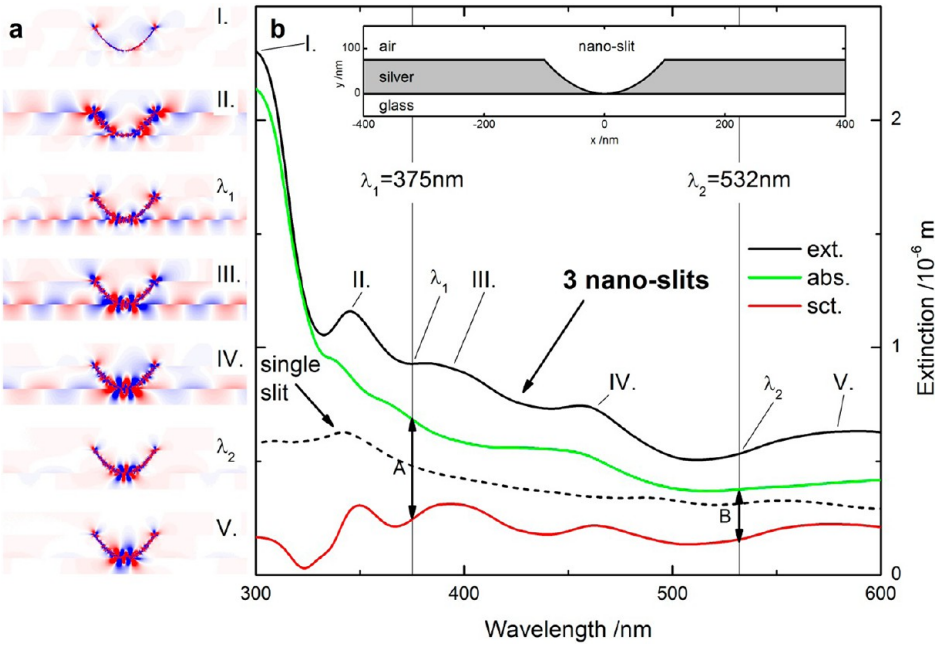

Figure 4. Surface charge distribution and extinction cross-section simulated for a single nanoslit (dashed line) and three nanoslits (solid lines). (a) Surface charge distribution of the main plasmonic modes (blue for negative, red for positive charges) at the glass−metal−air interface of the center nanoslit. (b) Dependence of the extinction (black curve), absorption (green), and scattering (red) of the light on wavelength. The calculations are presented for seven different wavelength marked in b (I = 300 nm, II = 345 nm, λ_1 = 375 nm, III = 395 nm, IV = 460 nm, λ_2 = 532 nm, V =580 nm).

detectable using AFM despite the presence of the polymer layer since a residual profile is created after deposition of the polymer (Figure 1b).

We irradiated the fabricated polymer−metal system with two different wavelengths of 375 and 532 nm. The wavelengths were chosen according to the absorption spectra of the polymer (see Figure S-1 in the Supporting Information). The 375 nm wavelength is close to the absorption peak of the polymer at 420 nm which initiates the photoisomerization (trans−cis transition) reaction, whereas the absorption at 532 nm is much weaker and does not induce photoisomerization easily.[26]

First, we performed light irradiation of the polymer−metal slit system at a polarization perpendicular to the nanoslits. For both wavelengths there is a change of the topography of the photosensitive polymer film, indicating a generation of a near-field surface pattern. However, the reaction of the polymer topography differ significantly (Figure 2). During irradiation with shorter wavelength of 375 nm, the polymer topography shows an increase in polymer thickness between the nanoslits. Compare to simulation a surface plasmon wave are excited at the curvature of the nanoslits. As we discuss later in more detail, this excited surface plasmon wave is highly damped and has a propagation length which is too short to form an interference. Consequently, we observe the dissipated energy of the surface plasmons between the nanoslits.

In the case of irradiation with 532 nm, a fine structuring of the polymer topography between the nanoslits becomes visible in AFM images (Figure 2b). The height of the generated periodic features is 5 nm and the periodicity is 170 nm, which is three times less than the wavelength of incoming light similarly to that reported earlier.[22] The depth is measured between the minimum polymer topography at the center of the nanoslit and the close by maximum above the nanoslit (see cross-section in Figure 2a). A video of topography changes during irradiation is available in the Supporting Information (Video S-1).

Figure 2c shows the distribution of the near-field intensity in the sample at the 375 nm wavelength calculated using FDTD simulations. The surface plasmon waves excited at the surface of the nanoslits are damped strongly near their edges and prevent propagation along the metal−polymer interface. In the case of irradiation with light of the 532 nm wavelength, the surface plasmon waves generated in the nanoslits interfere and result in a subdiffraction pattern. This periodicity and orientation of the interference pattern was confirmed by FDTD simulations which confirm that the interference pattern observed here is generated through the superposition of two counter-propagating surface plasmonic waves excited at the neighboring slits as has been suggested earlier (Figure 2d).[23]

Changing the polarization of incoming light to be parallel to the direction of nanoslits resulted in complete change of the observed phenomenon as supported by the calculated surface plasmon distribution. AFM images show that the polymer fills into the nanoslits under this illumination condition (Figure 3). The change in polymer topography is governed in this case by ordinary transmitted light, as supported by simulation results showing the distribution of electrical field intensity at the polymer side (Figure 3c, d). This means for the same nanostructure, the topography pattern can be almost inverted in the case of the 532 nm wavelength. An inverted pattern in this context implies a topography change from a periodic interference pattern to a topography pattern exactly above the nanoslits. It was previously shown that the direction of mass migration of the polymer material is toward light intensity and that is observed here as well.[20] In contrast, the polymer film topography was almost completely flattened after irradiation with the 375 nm wavelength (Figure 3c). This change can be explained by the fact that the polymer absorbs more at the shorter wavelength than at 532 nm, which results in a stronger photoisomerization reaction of azobenzene molecules and thus

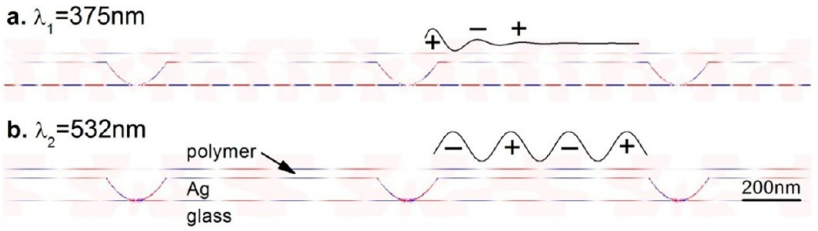

Figure 5. Surface charge distribution of two slit modes generated at (a) 375 and (b) 532 nm wavelength. The surface plasmon polaritons are propagating along the interfaces shown by the positive (red) and negative (blue) charges. The inserted intensity field illustrates the damped plasmon waves at 375 nm and the interference of two counter-propagating polaritons at 532 nm with the polymer−air interface acting as a specific dielectric waveguide.

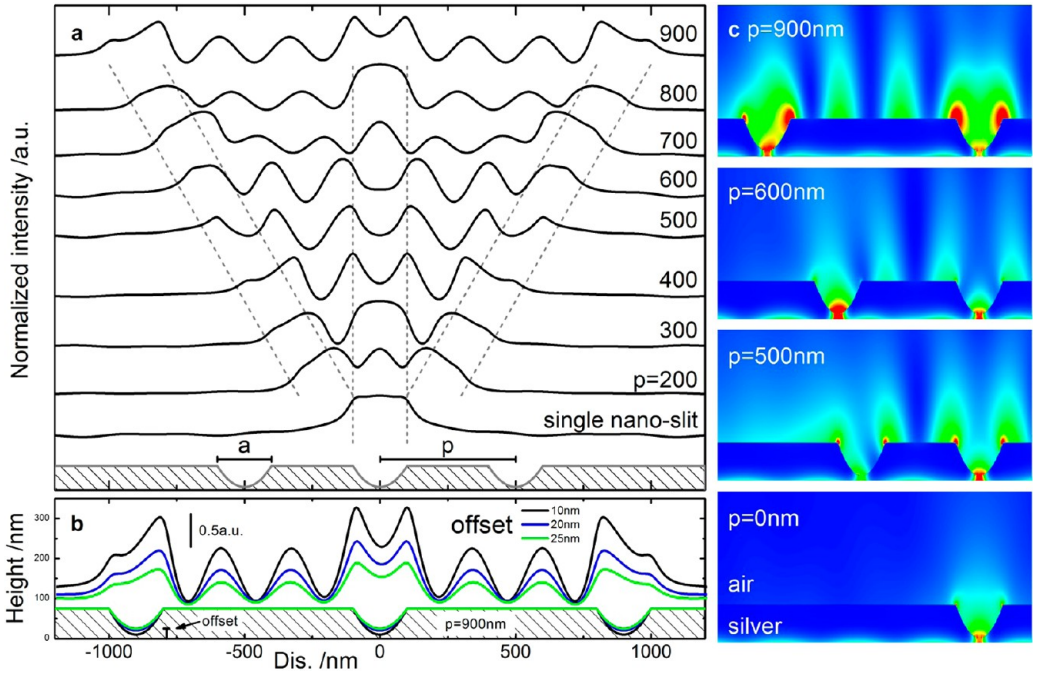

Figure 6. FDTD simulation of the intensity field at different nanoslit periods (p = 0−900 nm). (a) Profile of the near-field intensity distribution above the three nanoslits monitored at a 70 nm distance to the silver layer. The position of the nanoslits relative to the intensity profile is marked by the dashed lines. (b) Intensity patterns at three different thicknesses of the metal left at the bottom of nanoslits (offset): 10 nm (black curve), 20 nm (blue curve), 25 nm (green curve). The period and the aperture of the nanoslits are constant at 900 and 200 nm, respectively. (c) Intensity distributions of four selected periodicities. All intensity plots have the same color scale ranging from 0 (blue) to 2 au (red).

more pronounced mass transport of the polymeric material (see Figure S-1 in the Supporting Information).

To gain insight into the phenomenon, simulations of the surface charge distribution at the glass-metal-air interfaces as a function of the incoming wavelength were conducted without taking into account the presence of the azobenzene layer (Figure 4a). We chose a simple glass−silver−air setup, recorded the cross-section inside the source injection area (absorption), and recorded the radiation outside this area (scattering). The extinction cross-section is defined as the sum of the absorption cross-section and the scattering cross-section. The source injection area is defined by the nanostructure, the adjacent air layer, and the glass layer. The collective oscillation of surface charges results in electromagnetic fields that are bound to a glass-metal interface or to a metal-air interface and both decay exponentially. Depending upon conditions, different intensity patterns are generated as clarified by simulations.

Figure 4b represents the extinction cross-section calculated of the single and three neighboring nanoslits as a function of incoming wavelength. Five plasmon modes are revealed by these calculations inside the bandwidth between the 300 and 600 nm wavelengths (Figure 4b). Mode I at 300 nm wavelength is characterized by strong absorption, which is illustrated by a strong confinement of the surface charges at the nanoslit center (Figure 4a). This mode is likely caused by bound electrons and interband transitions. With an increase in wavelength, the amount of absorption decreases exponentially, whereas the scattering remains relatively constant. Consequently, the ratio between scattering and absorption increases with wavelength. This ratio is labeled as A and B in Figure 4b. This higher amount of scattering scaled by the absorption at longer wavelengths could explain the better radiation of the surface plasmon wave at 532 nm wavelength.

Additionally, we simulated the extinction cross-section of a single nanoslit to represent the noninterference case (dashed line in Figure 4b). Essentially, one plasmon mode could be excited in the noninterference case that corresponds in the wavelength position with mode II from the three nanoslit setup. From comparison with the noninterference case, we can assume that the modes between II and V are caused by

dx.doi.org/10.1021/am400712r | ACS Appl. Mater. Interfaces 2013, 5, 6009−6016

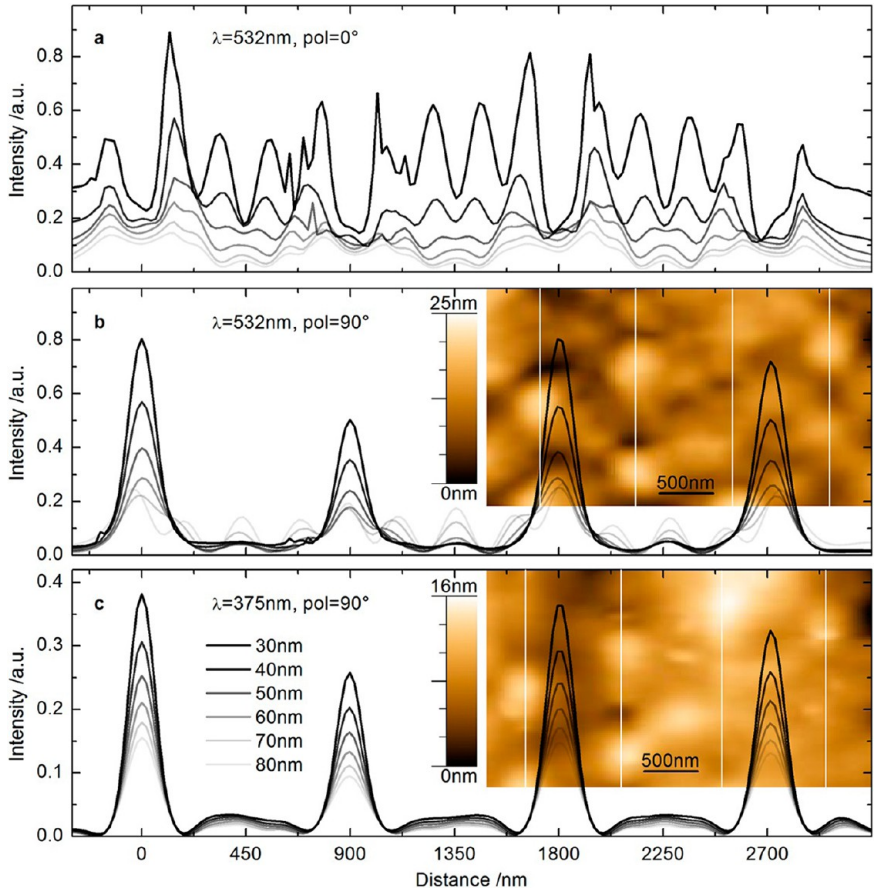

Figure 7. FDTD simulations of the intensity distribution as a function of polymer film thickness. The results are presented for the irradiation with 532 nm wavelength of (a) perpendicular and (b) parallel polarization to the nanoslits and (c) for the wavelength of 375 nm with a polarization parallel to the nanoslits. AFM images of the polymer film after irradiation with 532 and 375 nm are inserted in b and c respectively.

interference phenomenon. This kind of interference could occur either at the glass-silver interface or at the silver-air interface. Consequently, at 375 nm wavelength, we experimentally observed a slit mode of strongly damped plasmonic waves at the metal−air interface with a propagation length too short for an interference.

This claim is much more apprent if we include the polymer film of 30 nm thickness in the FDTD simulations (Figure 5). The charge plots displays significant damping at 375 nm and the interference of the two counter-propagating surface plasmon waves excited at the metal−polymer interface at 532 nm. Becaues of the index shift between polymer and air, the polymer−air interface acts as a dielectric waveguide.

Not only the wavelength of incoming light, but also the periodicity of the nanoslits influences the distribution of near-fields significantly. Figure 6 shows the results of near-field intensity pattern simulations at the metal-air interface generated at parallel nanoslit arrays with different periodicities. As a starting point, a single nanoslit was considered while illuminated with light of wavelength λ = 532 nm from the glass side. For 200 to 500 nm periodicity, the pattern intensity is dominated by the nanoslit edges. The intensity plots for the periodicity greater than 500 nm show clear interference patterns caused by two counter-propagating plasmonic waves at the metal-air interface (see Video S-2 in the Supporting Information).

Interestingly, the period of the interference pattern for periodicities from 600 to 900 nm is approximately constant at 260 ± 6 nm. Furthermore, in respect to the intensity distribution, two different plasmonic slit modes could be observed at the nanoslit corner and center, highlighted by the hot-spots as shown in Figure 6c and the plasmonic coupling between the nanoslit centers appears at 600 nm periodicity. The highest intensity at the metal−air interface could be found when a small metal layer is present in the nanoslit center (offset parameter in Figure 6b, this simulation is done for 900 nm periodicity only). We have found that the metal does not significantly alter the intensity and shape of the SP pattern at the metal−air interface up to a thickness of 10 nm.

Finally, we analyzed how the thickness of the polymer film influences the near-field intensity distribution at the polymer−air interface (Figure 7). In the case of the longer wavelength of 532 nm and polarization pointing perpendicular to the nanoslit, the amplitude of the plasmonic-generated interference pattern decreases exponentially with increasing film thickness (Figure 7a). The four positions of the interference pattern resulting from the standing plasmonic wave are visible for polymer films below 60 nm thickness. The profile of the intensity pattern is highly irregular because of the fact that in the simulation, the uneven geometry of real slits was utilized (derived from AFM images). In the case of polarization parallel to the nanoslit, the transmitted intensity decreases exponentially above the nanoslits as well, while starting from a polymer thickness of 50 nm, additional intensity peaks between nanoslits arose due to scattered light (Figure 7b). At a thickness of 80 nm, the polymer material flows into the nanoslits and smoothes the

dx.doi.org/10.1021/am400712r | ACS Appl. Mater. Interfaces 2013, 5, 6009−6016

surface, but the appearance of the additional peaks results in a rough polymer topography as shown in Figure 7b. Similar behavior was observed for the shorter wavelength and a polarization parallel to the nanoslit (Figure 7c). The inset AFM images illustrate the topography change after about 50 min of illumination. The amount of polymer that flowed into the nanoslits is not consistent because of the fact that residual Ag in the slits blocked the light in some areas. This residual Ag is left over from the AFM lithography slit fabrication.[25,33]

CONCLUSIONS

In summary, we analyzed the modulations of photosensitive polymer films which are induced by surface plasmonic interference generated by the nanoslit arrays fabricated in a silver layer. The fine polymer film topography with subdiffraction modulations exactly follow the calculated light intensity pattern, which strongly depends on the wavelength and polarization of incoming light. We observed that the topographical modulations can be excited only when the polarization is perpendicular to the nanoslits. Moreover, we have shown that irradiation with certain wavelengths resulted in a characteristic topographical pattern with the periodicity three times smaller than the wavelength of incoming light. FDTD simulations demonstrated that the unique subdiffraction topographical patterns are caused by constructive interference between two counter-propagating surface plasmon waves generated at neighboring nanoslits in the metal layer beneath the photosensitive polymer nanofilm with parameters and appearance predictably controlled by light wavelength, polarization orientation, and polymer film thickness.

We suggest that the symmetry, periodicity, and global shape of submicrometer-patterned polymer films can be further extended beyond simple patterns considered here by designing shape-controlled metal nanostructures beneath the polymer films such as checkerboard or bull-eyes structures. The approach discussed here can be used for prospective applications in designing high-resolution complex substrates, such as optical gratings, with widely variable and finely controlled optical properties. Furthermore this approach could be used for controllable surface nanoroughness, adhesion, wettability, surface stiffness, and biomolecular adsorption.

ASSOCIATED CONTENT

Supporting Information

Absorption spectrum and chemical structure of azobenzene polymer, schematic diagram of AFM experimental setup, video of the in situ recorded topography deformation during irradiation, and video showing FDTD simulation of different near-field intensity pattern distribution as a function of irradiation time and periodicity of the nanoslits. This material is available free of charge via the Internet at http://pubs.acs.org.

AUTHOR INFORMATION

Corresponding Author

*E-mail: santer@uni-potsdam.de.

Notes

The authors declare no competing financial interest.

ACKNOWLEDGMENTS

This research is supported by the DFG (SA1657/4-1) and U.S. Department of Energy, Office of Basic Energy Sciences, Division of Materials Sciences and Engineering under Award # DE-FG02-09ER46604 (simulations). We thank Dr. J. Stumpe and Dr. L. M. Goldenberg from the Fraunhofer Institute for Applied Polymer Research, Golm, Germany for providing the photosensitive polymer. We thank Jeffrey A. Geldmeier for proofreading of this manuscript.

REFERENCES

(1) Ichimura, K.; Oh, S.-K.; Nakagawa, M. *Science* **2000**, *288*, 1624−1626.
(2) Hall, R.; Hara, M.; Knoll, W. *Langmuir* **1996**, *12*, 2551−2555.
(3) Ullal, C. K.; Maldovan, M.; Wohlgemuth, M.; Thomas, E. L.; White, C. A.; Yang, S. *J. Opt. Soc. Am. A* **2003**, *20*, 948−954.
(4) Jang, J.-H.; Ullal, C. K.; Gorishnyy, T.; Tsukruk, V. V.; Thomas, E. L. *Nano Lett.* **2006**, *6*, 740−743.
(5) Jang, J.-H.; Ullal, C. K.; Choi, T.; Lemieux, M. C.; Tsukruk, V. V.; Thomas, E. L. *Adv. Mater.* **2006**, *18*, 2123−2127.
(6) Luo, X.; Ishihara, T. *Appl. Phys. Lett.* **2004**, *84*, 4780−4783.
(7) Srituravanich, W.; Fang, N.; Sun, C.; Luo, Q.; Zhang, X. *Nano Lett.* **2004**, *4*, 1085−1088.
(8) Liu, S.; Cheng, M.; Yang, Z.; Wang, Q. *Opt. Lett.* **2008**, *33*, 851−853.
(9) Shao, D. B.; Chen, S. C. *Nano Lett.* **2006**, *6*, 2279−2283.
(10) Guo, X.; Du, J.; Guo, Y.; Yao, J. *Opt. Lett.* **2006**, *31*, 2613−2615.
(11) Barnes, W. L.; Dereux, A.; Ebbesen, T. W. *Nature* **2003**, *424*, 824−830.
(12) Raether, H.*Surface Plasmons on Smooth and Rough Surfaces on Gratings*; Spring Tracts on Modern Physics; Springer: Berlin, 1988; Vol. *111*, p 136.
(13) Pitarke, J. M.; Silkin, V. M.; Chulkov, E. V.; Echenique, P. M. *Rep. Prog. Phys.* **2007**, *70*, 1−87.
(14) Salerno, M.; Felidj, N.; Krenn, J. R.; Leitner, A.; Aussenegg, F. R. *Phys. Rev. B* **2001**, *63*, 165422.
(15) Bouhelier, A.; Huser, T.; Hamaru, H.; Guntherodt, H. J.; Pohl, D. W.; Baida, F. I.; Van Labeke, D. *Phys. Rev. B* **2001**, *63*, 155404.
(16) Hillenbrand, R.; Keilmann, F.; Hanarp, P.; Sutherland, D. S.; Aizpurua, J. *Appl. Phys. Lett.* **2003**, *83*, 368−370.
(17) Shao, D. B.; Chen, S. C. *Appl. Phys. Lett.* **2005**, *86*, 253107.
(18) Juan, M. L.; Plain, J.; Bachelot, R.; Royer, P.; Gray, S. K.; Wiederrecht, G. P. *ACS Nano* **2009**, *3*, 1573−1579.
(19) Derouard, M.; Hazart, J.; Lérondel, G.; Bachelot, R.; Adam, P.-M.; Royer, P. *Opt. Express* **2007**, *15*, 4238−4246.
(20) König, T.; Goldenberg, L. M.; Kulikovska, O.; Kulikovsky, L.; Stumpe, J.; Santer, S. *Soft Matter* **2011**, *7*, 4174−4178.
(21) Hubert, C.; Rumyantseva, A.; Lerondel, G.; Grand, J. S.; Kostcheev, L.; Billot, Vial, A.; Bachelot, R.; Royer, P.; Chang, S. H.; Gray, S. K.; Wiederrecht, G. P.; Schatz, G. C. *Nano Lett.* **2005**, *5*, 615−619.
(22) König, T.; Santer, S. *Nanotechnology* **2012**, *23*, 155301 8pp..
(23) König, T.; Sekhar, Y. N.; Santer, S. *J. Mater. Chem.* **2012**, *22*, 5945−5950.
(24) König, T.; Sekhar, Y. N.; Santer, S. *Plasmonics* **2012**, *7*, 535−542.
(25) König, T.; Santer, S. *Nanotechnology* **2012**, *23*, 485304 7pp..
(26) Rochon, P.; Batalla, E.; Natansohn, A. *Appl. Phys. Lett.* **1995**, *66*, 136−139.
(27) Kim, D. Y.; Tripathy, S. K.; Li, L.; Kumar, J. *Appl. Phys. Lett.* **1995**, *66*, 1166−1169.
(28) Kim, D. Y.; Li, L.; Jiang, X. L.; Shivshankar, V.; Kumar, J.; Tripathy, S. K. *Macromolecules* **1995**, *28*, 8835−8839.
(29) Rabek, J. F. *Progress in Photochemistry and Photophysics*; CRC Press: Boca Raton, FL, 1991, 216.
(30) Barrett, C. J.; Rochon, P. L.; Natansohn, A. L. *J. Chem. Phys.* **1998**, *109*, 1505−1517.
(31) Kumar, J.; Li, L.; Jiang, X. L.; Kim, D.-Y.; Lee, T. S.; Tripathy, S. *Appl. Phys. Lett.* **1998**, *72*, 2096−2099.
(32) Baldus, O.; Zilker, S. J. *Appl. Phys. B: Laser Opt.* **2001**, *72*, 425−427.

(33) König, T.; Papke, T.; Kopyshev, A.; Santer, S. *J. Mater. Sci.* **2013**, *48*, 3863−3869.
(34) Kulikovska, O.; Goldenberg, L. M.; Stumpe. *Chem. Mater.* **2007**, *19*, 3343−3348.
(35) Hagemann, H. J.; Gudat, W.; Kunz, C. *J. Opt. Soc. Am.* **1975**, *65*, 742−744.
(36) Palik, E. D. *Handbook of OPtical Contstants in Solids*; Academic Press: New York, 1991; p 2.